Electronic Structure and Chemical Bonding of Transition-Metal Monoborides

Subjects: Chemistry, Physical

Contributor: Constantinos Demetriou , Christina Eleftheria Tzeliou , Alexandros Androutsopoulos , Demeter Tzeli

Boron presents an important role in chemistry, biology, and materials science. Diatomic transition-metal borides (MBs) are the building blocks of many complexes and materials, and they present unique electronic structures with interesting and peculiar properties and a variety of bonding schemes which are analyzed here. Comparisons between MB molecules along the three rows are presented, and their differences and similarities are analyzed. The bonding of the diatomic borides is also described. Three of them RhB($X^1\Sigma^+$), RuB($X^2\Delta$) and TcB($X^3\Sigma^-$) form quadruple $\sigma^2\sigma^2\pi^2\pi^2$ bonds in their X states. The RhB form quadruple bond also in two low-lying excited states.

Chemical Bonding Transition Metal Boride Electronic structure Calculations

1. Introduction

Boron has an important role in chemistry, biology, and materials science [1]. It is well known that it forms single, double, and triple bonds, but it was only recently found that it can form quadruple bonds in specific diatomic molecules [2][3][4][5]. Additionally, its chemistry is quite interesting to preparative chemists, theoreticians, industrial chemists, and technologists. It is noteworthy that it is the only non-metal in group 13 of the periodic table, and it presents many similarities to its neighbor, carbon, and its diagonal relative, silicon. Hence, like C and Si, it showcases a marked propensity to form covalent, molecular compounds, but it differs greatly from them in having one less valence electron, a situation sometimes referred to as “electron deficiency”. This deficiency plays a key role in its chemistry [1].

Transition-metal borides have received considerable attention since they present common catalytic properties for the hydrogenation of alkenes and alkynes, the reduction of nitrogenous functional groups, and deoxygenation reactions [6]. They are important building blocks in many complexes and materials. Moreover, they possess remarkable physical properties, such as very high conductivity (TiB_2) [7]—even superconductivity (MgB_2) [8]—as well as super hardness (ReB_2) [9]. In solid state, many computational and experimental studies have been carried out; see, for instance, [10][11][12][13][14][15][16][17][18]. Computationally, the DFT methodology is applied to determine the bond lengths, frequencies, and vibrational properties of solids [10][13]; density of state; bond population; charge density maps [14]; relative stability; mechanical, electronic, and magnetic properties [15]; elastic behavior; and elastic anisotropy [16]. Furthermore, ab initio molecular dynamic (AIMD) simulations at finite temperature have also been employed in order to investigate the structural stability of materials, for instance, those of U_2B (U = Ti, Cr, Nb, Mo, Ta, and W) [18].

It has been reported that the electronic structure and the chemical bonding of diatomic and triatomic molecules are strongly related to their structure, the variety of their morphologies, and the properties of their 2D- materials and solid state [19][20]. Therefore, an investigation of the electronic structure and the bonding of the diatomic transition-metal borides, which constitute the simplest building blocks of the compounds or materials in question, would lay the foundation for understanding the very complex solid-metal borides and even their bulk properties. Finally, it should be noted that the diatomic transition-metal borides showcase unique electronic structures presenting interesting and peculiar properties and a variety of bonding schemes.

The present entry is adapted from Ref [21], where presents the bond distances, dissociation energies, frequencies, dipole moments, and natural NPA charges of all three rows transition-metal borides. Here the comparisons between the MB molecules of all three rows are presented, and their differences and similarities are analyzed. Finally, transition-metal borides forming quadruple bonds are described and analyzed here, and for the first time, we report on the RuB and TcB molecules.

2. Transition Metals Monoborides

Quantum chemical computations provide details on the chemical bonds and electronic structures of these species. In general, the bond lengths of the transition-metal borides increase in the periodic table from left to right, or as one goes down a group of elements. Of course, anomalies occur, but the data are the result of the variety of bonding schemes that are formed in the MB molecules. These bonding schemes depend on the bonding and the filling of σ, π, and δ orbitals. MBs can form one-and-a-half, double, triple, and even quadruple bonds, with the latter being recently discovered in RhB and RhB^- [2][4][5], while here, we found that RuB and TcB also form quadruple bonds.

The bond distances of the ground states of the MBs of all three rows, with respect to the different M atoms, are plotted in **Figure 1a**. Moving from up (first row) to down (third row) the bond distances, in the cases with the same bonding, the r_e values increase by about 1 Å. Also, moving from left to right, the r_e value decreases up to the seventh or eighth MB, and then the r_e value increases sharply. All differences are a result of the type of bonding. In all rows, there are three MBs that present similar strong bonding. Thus, along the first row, from the sixth to the eighth MB, i.e., FeB, CoB, and NiB, a triple bond and similar r_e values, around 1.7 Å, are observed. Similarly, along the third row, from the sixth to the eighth MB, OsB, IrB, and PtB, a triple bond and similar r_e values, around 1.76 Å, are found. On the contrary, in the second row, from the fifth to the seventh MB, i.e., TcB, RuB, and RhB, a quadruple bond is formed with similar r_e values, around 1.7 Å.

In **Figure 1d,e**, the dissociation energies with respect to the adiabatic products (D_e) and the atomic ground state products at the zero-vibrational level ($D_{0,GS}$) are plotted with respect to the change in the M atom from left to right for the three rows. The general shape is the same as that of the lowest dissociation energies being observed for the M, with atomic configurations of $(ds)^6$ or $(ds)^7$ and $d^{10}s^2$, while the highest values are observed for the M with atomic configurations of $(ds)^{8–10}$ for the first and third rows and $(ds)^{7–9}$ for the second row, and the largest values are found for the second and third rows. Finally, it should be noted that the first two and the last two MBs present similar dissociation energy regardless of the row.

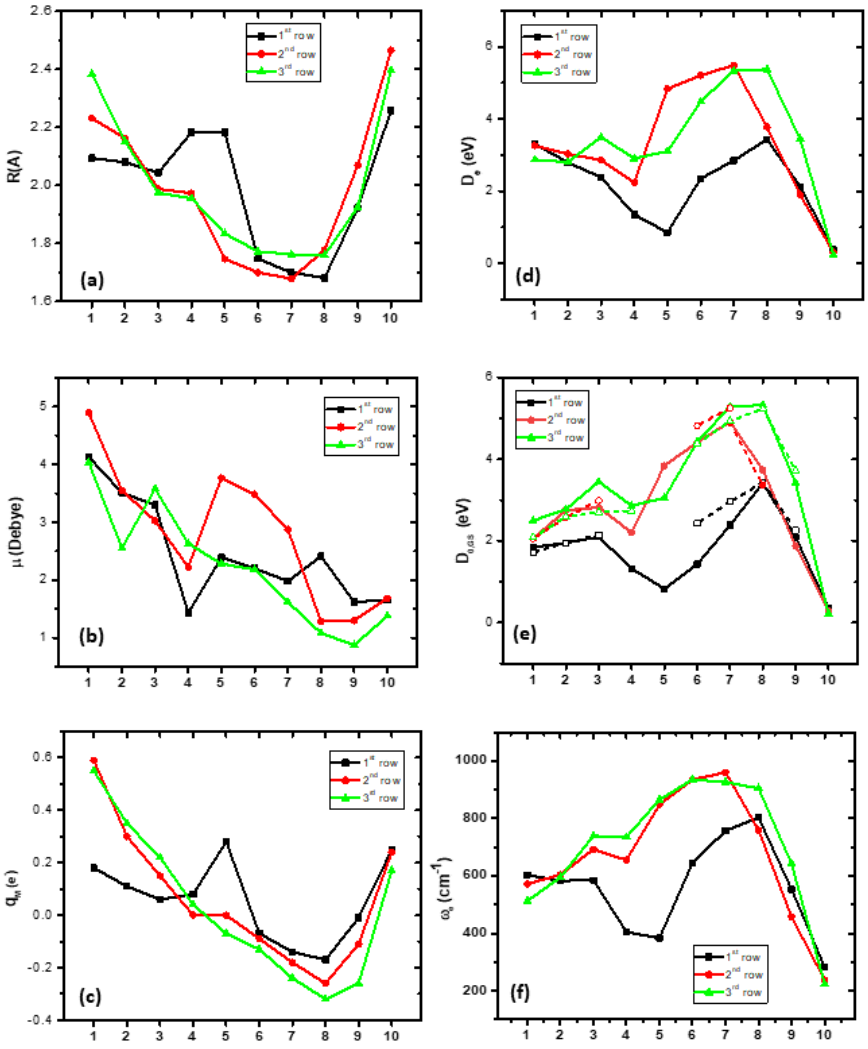

Figure 1. (**a**) Bond lengths, r_e, (**b**) dipole moments, μ, (**c**) charge on metal, q_M, via natural population analysis, (**d**) dissociation energies, D_e (eV), with respect to the adiabatic atomic products, (**e**) dissociation energies, $D_{0,GS}$, with respect to the ground state atomic products, and (**f**) vibrational frequencies, ω_e, of the ground states of the 1st-, 2nd-, and 3rd-row-transition-metal boride molecules; 1st row: MRCISD+Q/aug-cc-pV5Z [22]; 2nd- and 3rd-row MBs: B3LYP/aug-cc-pVQZ$_B$(-PP)$_M$ and def2-QZVPPD$_{La}$ levels of theory [21].

The dipole moment, μ, with respect to the M follows roughly the same trend as the M changes from left to right in each row, i.e., a general reduction in the μ value. Any differences are related to the differences in the bonding; see **Figure 1b**. The smallest differences among the three rows are observed in d^1s^2, $(ds)^5$, and $d^{10}s^2$, while the first and third rows present similar μ values for the d^5s^2 metals, where the second-row MB presents a μ value larger by 1.5 D than the corresponding MnB and ReB values due to the quadruple bond of TcB.

Table 1. Atomic states of transition metals forming the bonding (in situ M) of the ground MB state (X) and the atomic state of M in $R_{M\text{-}B}$ infinity; and of the atomic ground state X_M and the energy difference between the ground atomic state and the atomic state forming the bonding T_e (eV) (M_J-averaged experimental).

MB	X	Configuration	Bond	In Situ M	In R_{M-B} Infinity	X_M	T_e [b]
		1st row		MB		M	
ScB	$X^5\Sigma^-$	$1\sigma^2 2\sigma^1 3\sigma^1 1\pi^1 1\pi^1$	$\sigma^1\pi_x^1\pi_y^1$	$^4F[3d^2 4s^1]$ [a]	$^4F[3d^2 4s^1]$	$^2D[3d^1 4s^2]$	1.428(1.427)
TiB	$X^6\Delta$	$1\sigma^2 2\sigma^1 3\sigma^1 1\pi^1 1\pi^1 1\delta^1$	$\sigma^1\pi_x^1\pi_y^1$	$^5F[3d^3(^4F)4s^1]$ [a]	$^5F[3d^3(^4F)4s^1]$	$a^3F[3d^2 4s^2]$	0.813(0.806)
VB	$X^7\Sigma^+$	$1\sigma^2 2\sigma^1 3\sigma^1 1\pi^1 1\pi^1 1\delta^1 1\delta^1$	$\sigma^1\pi_x^1\pi_y^1$	$^6D[3d^4(^5D)4s^1]$ [a]	$^6D[3d^4(^5D)4s^1]$	$a^4F[3d^3 4s^2]$	0.262(0.245)
CrB	$X^6\Sigma^+$	$1\sigma^2 2\sigma^2 3\sigma^1 1\pi^1 1\pi^1 1\delta^1 1\delta^1$	$\sigma^2\pi_x^1\pi_y^1$	$^7S[3d^5(^6S)4s^1]$ [a]	$^7S[3d^5(^6S)4s^1]$	$^7S[3d^5(^6S)4s^1]$	0
MnB	$X^5\Pi$	$1\sigma^2 2\sigma^2 3\sigma^1 1\pi^2 1\pi^1 1\delta^1 1\delta^1$	$\sigma^2\pi_x^2\pi_y^1$	$^6S[3d^5 4s^2]$ [a]	$^6S[3d^5 4s^2]$	$a^6S[3d^5 4s^2]$	0
FeB	$X^4\Sigma^-$	$1\sigma^2 2\sigma^2 3\sigma^1 1\pi^2 1\pi^2 1\delta^1 1\delta^1$	$\sigma^2\pi_x^2\pi_y^2$	$a^5F[3d^7(^4F)4s^1]$ [a]	$a^5D[3d^6 4s^2]$	$a^5D[3d^6 4s^2]$	0.859(0.875)
CoB	$X^3\Delta$	$1\sigma^2 2\sigma^2 3\sigma^1 1\pi^2 1\pi^2 1\delta^2 1\delta^1$	$\sigma^2\pi_x^2\pi_y^2$	$b^4F[3d^8(^3F)4s^1]$ [a]	$a^4F[3d^7 4s^2]$	$a^4F[3d^7 4s^2]$	0.432(0.417)
NiB	$X^2\Sigma^+$	$1\sigma^2 2\sigma^2 3\sigma^1 1\pi^2 1\pi^2 1\delta^2 1\delta^2$	$\sigma^2\pi_x^2\pi_y^2$	$a^3D[3d^9(^2D)4s^1]$ [a]	$a^3F[3d^8(^3F)4s^2]$	$a^3F[3d^8(^3F)4s^2]$	0.025(-0.030)
CuB	$X^1\Sigma^+$	$1\sigma^2 2\sigma^2 3\sigma^2 1\pi^2 1\pi^2 1\delta^2 1\delta^2$	$\sigma^2\pi_x^2\pi_y^2$	$^2S[3d^{10}(^1S)4s^1]$ [a]	$^2S[3d^{10}(^1S)4s^1]$	$^2S[3d^{10}(^1S)4s^1]$	0
		2nd row					
ZnB	$X^2\Pi$	$1\sigma^2 2\sigma^2 3\sigma^2 1\pi^2 1\pi^2 2\pi^1 1\delta^2 1\delta^2$	$\sigma^2\pi^2$	$^1S[3d^{10}4s^2]$	$^1S[3d^{10}4s^2]$	$^1S[3d^{10}4s^2]$	0
YB	$X^5\Sigma^-$	$1\sigma^2 2\sigma^1 3\sigma^1 1\pi^1 1\pi^1$	$\sigma^1\pi_x^1\pi_y^1$	$^4F[4d^2 5s^1]$	$a^4F[4d^2(^3F)5s]$	$a^2D[4d5s^2]$	1.356(1.359)

ZrB	***X*** $^{6}\Delta$	$1\sigma^2 2\sigma^1 3\sigma^1 1\pi^1 1\pi^1 1\delta^1$	$\sigma^1\pi_x^1\pi_y^1$	$^{5}F[4d^3(^4F)5s^1]$	$a^{5}F[4d^3(^4F)5s^1]$	$a^{3}F[4d^2 5s^2]$	0.604(0.588)
NbB	$^{5}\Pi/^{5}\Phi$	$1\sigma^2 2\sigma^1 3\sigma^1 1\pi^2 1\pi^1 1\delta^1$	$\sigma^1\pi_x^2\pi_y^1$	$a^{6}D[4d^4(^5D)5s^1]$	$a^{6}D[4d^4(^5D)5s^1]$	$a^{6}D[4d^4(^5D)5s^1]$	0
	$^{3}\Sigma^{+}$	$1\sigma^2 2\sigma^1 3\sigma^1 1\pi^2 1\pi^2$	$\sigma^1\pi_x^2\pi_y^2$	$a^{4}D[4d^4 5s^1]$	$a^{4}F[4d^3 5s^3]$	$a^{6}D[4d^4(^5D)5s^1]$	1.043(1.049)
MoB	$X^{6}\Pi$	$1\sigma^2 2\sigma^1 3\sigma^1 1\pi^2 1\pi^1 1\delta^1 1\delta^1$	$\sigma^1\pi_x^2\pi_y^1$	$a^{7}S[4d^5(^6S)5s]$	$a^{7}S[4d^5(^6S)5s]$	$a^{7}S[4d^5(^6S)5s]$	0
TcB	$X^{3}\Sigma^{-}$	$1\sigma^2 2\sigma^2 1\pi^2 1\pi^2 1\delta^1 1\delta^1$	$\sigma^2\sigma^2\pi_x^2\pi_y^2$	$^{4}F[4d^7]$	$^{4}D[4d^6(^5D)5s]$	$^{6}S[4d^5 5s^2]$	1.827(2.332)
	$^{5}\Sigma^{-}$	$1\sigma^2 2\sigma^1 3\sigma^1 1\pi^2 1\pi^2 1\delta^1 1\delta^1$	$\sigma^1\pi_x^2\pi_y^2$	$^{6}D[4d^6 5s^1]$	$^{6}S[4d^5 5s^2]$	$^{6}S[4d^5 5s^2]$	0.319(0.406)
	$^{7}\Sigma^{-}$	$1\sigma^2 2\sigma^1 3\sigma^1 1\pi^2 1\pi^1 2\pi^1 1\delta^1 1\delta^1$	$\sigma^1\pi^1$	$^{6}D[4d^6 5s^1]$	$^{6}S[4d^5 5s^2]$	$^{6}S[4d^5 5s^2]$	0.319(0.406)
RuB	$X^{2}\Delta$	$1\sigma^2 2\sigma^2 1\pi^2 1\pi^2 1\delta^2 1\delta^1$	$\sigma^2\sigma^2\pi_x^2\pi_y^2$	$b^{3}F[4d^8]$	$a^{3}F[4d^7(a^4F)5s]$	$a^{5}F[4d^7(a^4F)5s]$	1.131(1.092)
RhB	$X^{1}\Sigma^{+}$	$1\sigma^2 2\sigma^2 1\pi^2 1\pi^2 1\delta^2 1\delta^2$	$\sigma^2\sigma^2\pi_x^2\pi_y^2$	$a^{2}D[4d^9]$	$a^{2}D[4d^9]$	$a^{4}F[4d^8(^3F)5s]$	0.410(0.342)
PdB	$X^{2}\Sigma^{+}$	$1\sigma^2 2\sigma^2 3\sigma^1 1\pi^2 1\pi^2 1\delta^2 1\delta^2$	$\sigma^2\pi_x^2\pi_y^2$	$^{1}S[4d^{10}]$	$^{1}S[4d^{10}]$	$^{1}S[4d^{10}]$	0
AgB	$X^{1}\Sigma^{+}$	$1\sigma^2 2\sigma^2 3\sigma^2 1\pi^2 1\pi^2 1\delta^2 1\delta^2$	$\sigma^2\pi_x^2\pi_y^2$	$^{2}S[4d^{10}5s]$	$^{2}S[4d^{10}5s]$	$^{2}S[4d^{10}5s]$	0
CdB	$X^{2}\Pi$	$1\sigma^2 2\sigma^2 3\sigma^2 1\pi^2 1\pi^2 2\pi^1 1\delta^2 1\delta^2$	$\sigma^2\pi^2$	$^{1}S[4d^{10}5s^2]$	$^{1}S[4d^{10}5s^2]$	$^{1}S[4d^{10}5s^2]$	0
		3rd row					
LaB	$X^{5}\Sigma^{-}$	$1\sigma^2 2\sigma^1 3\sigma^1 1\pi^1 1\pi^1$	$\sigma^1\pi_x^1\pi_y^1$	$^{4}F[5d^2(^3F)6s]$	$^{4}F[5d^2(^3F)6s]$	$^{2}D[5d6s^2]$	0.331(0.355)
	$^{3}\Pi$	$1\sigma^2 2\sigma^1 1\pi^2 1\pi^1$	$\sigma^1\pi_x^2\pi_y^1$	$b^{4}F[5d^3]$	$^{2}D[5d6s^2]$	$^{2}D[5d6s^2]$	1.541(1.560)

HfB	**$X^4\Sigma^-$**	$1\sigma^2 2\sigma^2 3\sigma^1 1\pi^1 1\pi^1$	$\sigma^1\pi_x^1\pi_y^1$	$a^3F[5d^26s^2]$	$a^3F[5d^26s^2]$	$a^3F[5d^26s^2]$	0
TaB	**$X^5\Delta$**	$1\sigma^2 2\sigma^1 3\sigma^1 1\pi^2 1\pi^1 1\delta^1$	$\sigma^1\pi_x^2\pi_y^1$	$a^6D[5d^46s^1]$	$a^4F[5d^36s^2]$	$a^4F[5d^36s^2]$	1.210(1.038)
	$^3\Sigma^+$	$1\sigma^2 2\sigma^1 3\sigma^1 1\pi^2 1\pi^2$	$\sigma^1\pi_x^2\pi_y^2$		$a^4F[5d^36s^2]$	$a^4F[5d^36s^2]$	
WB	**$X^6\Pi$**	$1\sigma^2 2\sigma^1 3\sigma^1 1\pi^2 1\pi^1 1\delta^1 1\delta^1$	$\sigma^1\pi_x^2\pi_y^1$	$^7S[5d^56s^1]$	$^5D[5d^46s^2]$	$^5D[5d^46s^2]$	0.366(−0.187)
	$^6\Sigma^+$	$1\sigma^2 2\sigma^2 3\sigma^1 1\pi^1 1\pi^1 1\delta^1 1\delta^1$	$\sigma^2\pi_x^1\pi_y^1$	$^7S[5d^56s^1]$	$^5D[5d^46s^2]$	$^5D[5d^46s^2]$	0.366(−0.187)
ReB	**$X^5\Sigma^-$**	$1\sigma^2 2\sigma^1 3\sigma^1 1\pi^2 1\pi^2 1\delta^1 1\delta^1$	$\sigma^1\pi_x^2\pi_y^2$	$a^6D[5d^66s^1]$	$a^6S[5d^56s^2]$	$a^6S[5d^56s^2]$	1.457(1.759)
	$^3\Sigma^-$	$1\sigma^2 2\sigma^2 1\pi^2 1\pi^2 1\delta^1 1\delta^1$	$\sigma^2\pi_x^2\pi_y^2$	$a^4P[5d^56s^2]$	$a^4P[5d^56s^2]$	$a^6S[5d^56s^2]$	1.436(1.603)
OsB	**$X^4\Sigma^-$**	$1\sigma^2 2\sigma^2 3\sigma^1 1\pi^2 1\pi^2 1\delta^1 1\delta^1$	$\sigma^2\pi_x^2\pi_y^2$	$a^5F[5d^7(^4F)6s^1]$	$a^5D[5d^66s^2]$	$a^5D[5d^66s^2]$	0.638(0.757)
IrB	**$X^3\Delta$**	$1\sigma^2 2\sigma^2 3\sigma^1 1\pi^2 1\pi^2 1\delta^2 1\delta^1$	$\sigma^2\pi_x^2\pi_y^2$	$a^4F[5d^76s^2]$	$a^4F[5d^76s^2]$	$a^4F[5d^76s^2]$	0
PtB	**$X^2\Sigma^+$**	$1\sigma^2 2\sigma^2 3\sigma^1 1\pi^2 1\pi^2 1\delta^2 1\delta^2$	$\sigma^2\pi_x^2\pi_y^2$	$^3D[5d^96s^1]$	$^3D[5d^96s^1]$	$^3D[5d^96s^1]$	0
AuB	**$X^1\Sigma^+$**	$1\sigma^2 2\sigma^2 3\sigma^2 1\pi^2 1\pi^2 1\delta^2 1\delta^2$	$\sigma^2\pi_x^2\pi_y^2$	$^2S[5d^{10}6s^1]$	$^2S[5d^{10}6s^1]$	$^2S[5d^{10}6s^1]$	0
HgB	**$X^2\Pi$**	$1\sigma^2 2\sigma^2 3\sigma^2 1\pi^2 1\pi^2 2\pi^1 1\delta^2 1\delta^2$	$\sigma^2\pi^2$	$^1S[5d^{10}6s^2]$	$^1S[5d^{10}6s^2]$	$^1S[5d^{10}6s^2]$	0
	$X^2\Sigma^+$	$1\sigma^2 2\sigma^2 3\sigma^2 4\sigma^1 1\pi^2 1\pi^2 1\delta^2 1\delta^2$	$(\pi^2\pi^2)$	$^1S[5d^{10}6s^2]$	$^1S[5d^{10}6s^2]$	$^1S[5d^{10}6s^2]$	0

[a] Ref. [21]. [b] Expt values of the energy separation between the term with the lowest in energy spin–orbit coupling angular momentum quantum number *J* (average term).

On the contrary, the NPA charge on the metals as the M changes from left to right has the same shape for all three rows apart, from the MnB of the first row; see Figure 1c. Finally, the change in the vibrational frequencies with

respect to M for the three rows has the same trend; see **Figure 1f**. In most MB molecules, the second- and third-row MBs have larger ω_e values than the MBs of the first row.

The dissociation energy per bond, i.e., per two bonding electrons, and the number of the formed bonds for all MBs of the first, second, and third rows are depicted in **Figure 2**. Regarding the diagram of the D_e/bond, the general shape is the same for all three rows. The largest D_e/bond, except for the first two and the last MBs, is observed for the MBs of the third row. Thus, the fact that the 4*d* series exhibits greater intrinsic bond energies [23] is explained with the formation of more multiple bonds than in some MBs of the 3*d* and 5*d* series, while the D_e/bond is the highest for the third row, as expected.

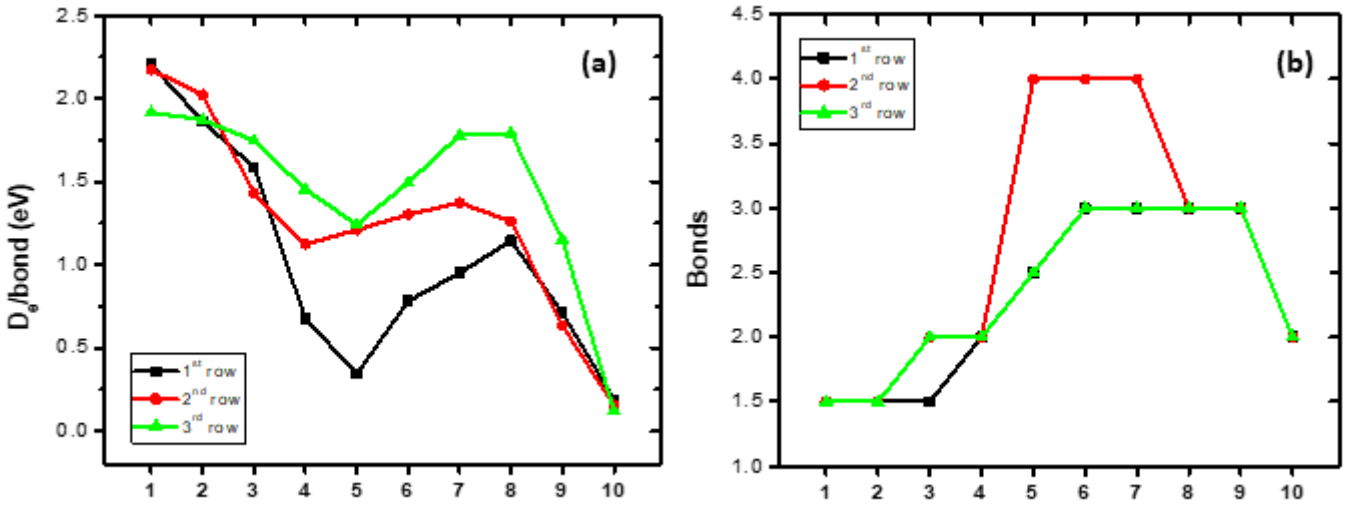

Figure 2. (**a**) Dissociation energies, D_e (eV), per bond with respect to the adiabatic atomic products; (**b**) number of formed bonds of the ground states of the 1st-, 2nd-, and 3rd-row-transition-metal boride molecules, MBs.

Regarding the number of bonds formed, it seems that the MB molecules of the first and third rows present the same multiple bonds, except the $(n)d^3(n + 1)s^2$ atoms, where, for VB, the ground state is $X^7\Sigma^+$ and for TaB it is $X^5\Delta$. The difference in spin multiplicities results in different orders of bonding. The largest observed difference between MBs of the second row with the corresponding MBs of the first and third rows is for the fifth MB, i.e., TcB (quadruple bond) vs MnB and ReB (two and a half bonds). Finally, the X states of the RuB and RhB molecules of the second row also have quadruple bonds, while the corresponding MB molecules of the other rows have triple bonds.

The formation of quadruple bonding in the MB part of the complexes has been reported in the literature. For instance, in the anionic complex $FeB(CO)_3^-$, a quadruple bond is formed in the FeB part. The $BFe(CO)_3^-$ anion was calculated via DFT and DLPNO-CCSD(T) methodologies and identified using mass-selected infrared photodissociation spectroscopy in the gas phase [24].

Finally, it should be noted that in the transition-metal molecules, highly correlated electrons are involved in the spin−orbit interactions, and relativistic effects exist. The use of basis sets with pseudopotentials of course simplified the complicated effects of the motion of the core (non-valence) electrons. Furthermore, 5*d* MB molecules suffer from strong spin−orbit effects, which have been neglected here. The use of atomic spin−orbit stabilization [25] may lead to reductions in the calculated dissociation energies [26]. However, our calculated values are in very good agreement with the experimental ones, with the exception of TaB, since both M and MB species are subject to the spin–orbit effects; thus, via the cancellation of errors, the D_e results are good. Specifically, our B3LYP/aug-cc-PVQZ(-PP) values are in better agreement with the experimental ones, and the energy differences between experimental and calculated values range from 0.046 (OsB) to 0.410 eV (LaB), apart from TaB, where the calculated value overestimates the experimental D_0 by 0.749 eV. On the contrary, for the second-row MBs, the energy differences between experimental and calculated values range from 0.002 eV to 0.343 eV. Finally, note that the main aim of the present study is to study the periodic bonding schemes and trends for MB molecules over three rows, providing a quantitative and qualitative picture of the chemical bonding in the MB species, which is presented here adequately.

3. Quadruple Bonding

In 2020, two works concerning the bonding structure of RhB were published, where the formation of a quadruple bond was reported. The first study conducted by Cheung et al. [2] explored the bonding nature of $RhB(BO)^-$ and RhB species via ADF, DFT, CCSD(T) methodologies. The second study, carried out by Tzeli and Karapetsas [4], investigated the bond occurring inside isoelectronic species between transition metals and the main group elements TcN, RuC, RhB and PdBe. For the RhB molecule, at various levels of theory, i.e., MRCISD, MRCISD+Q, and RCCSD(T)/aug-cc-pV5Z-PP_{Rh} aug-cc-pV5Z_B. Both studies found that the ground electronic state ($X^1\Sigma^+$) has a dominant $1\sigma^2 2\sigma^2 1\pi^4 1\delta^4$ configuration determinant and correlates adiabatically to the atomic electronic spin states B(X^2P;$2s^2 2p$) + Rh(a^2D;$4d^9$), resulting in a four-fold quadruple bond. Tzeli and Karapetsas [4] found that, except for the ground state of RhB, its two lowest excited states, i.e., $a^3\Delta$ and $A^1\Delta$, also present quadruple bonds [4]. Additionally, in the ground and the first excited states of the RhB^- anion, $X^2\Sigma^+$ and $A^2\Delta$ quadruple bonds are also formed [5].

Except from RhB($X^1\Sigma^+$), the TcB($X^3\Sigma^-$) and RuB($X^2\Delta$) also present quadruple bonds [21]. The bonding is formed from an atomic state which has an empty 5*s* orbital from, for example, Tc(^{4}F[$4d^7$]), Ru(b^3F[$4d^8$]), and Rh(a^2D[$4d^9$]). As a result, the 5*s* of the metal is empty and thus it can accept electrons, forming a dative bond. The bonding in *X* states is $1\sigma^2 2\sigma^2 1\pi_x^2 1\pi_y^2$; see Figure 3. Specifically, the bonding is $1\sigma^2$ = $(M4d_{z^2})^2 \rightarrow (B2p_z)^0$, which is a dative bond from the M to the B atom; $2\sigma^2$ = $(M5sM4d_{z^2})^0 \leftarrow (B2s)^2$, also a dative bond from the B to the M; and $1\pi_x^2$ = $(M4d_{xz})^1 - (B2p_x)^1$ and $1\pi_y^2$ = $(M4d_{yz})^1 - (B2p_y)^1$, which are both π covalent bonds. The similar bonding leads to similar short r_e values, smaller up to 0.3 Å with respect to MoB, and dissociation energies of about 5 eV (4.84 up to 5.49 eV). Note that there is a $5s5d_{z^2}$ hybridization in M and a $2s2p_z$ hybridization in B. The electrons added from Tc to Rh are added to non-bonding δ orbitals, i.e., $\delta^1\delta^1$ in TcB, $\delta^2\delta^1$ in RuB, and $\delta^2\delta^2$ in RhB.

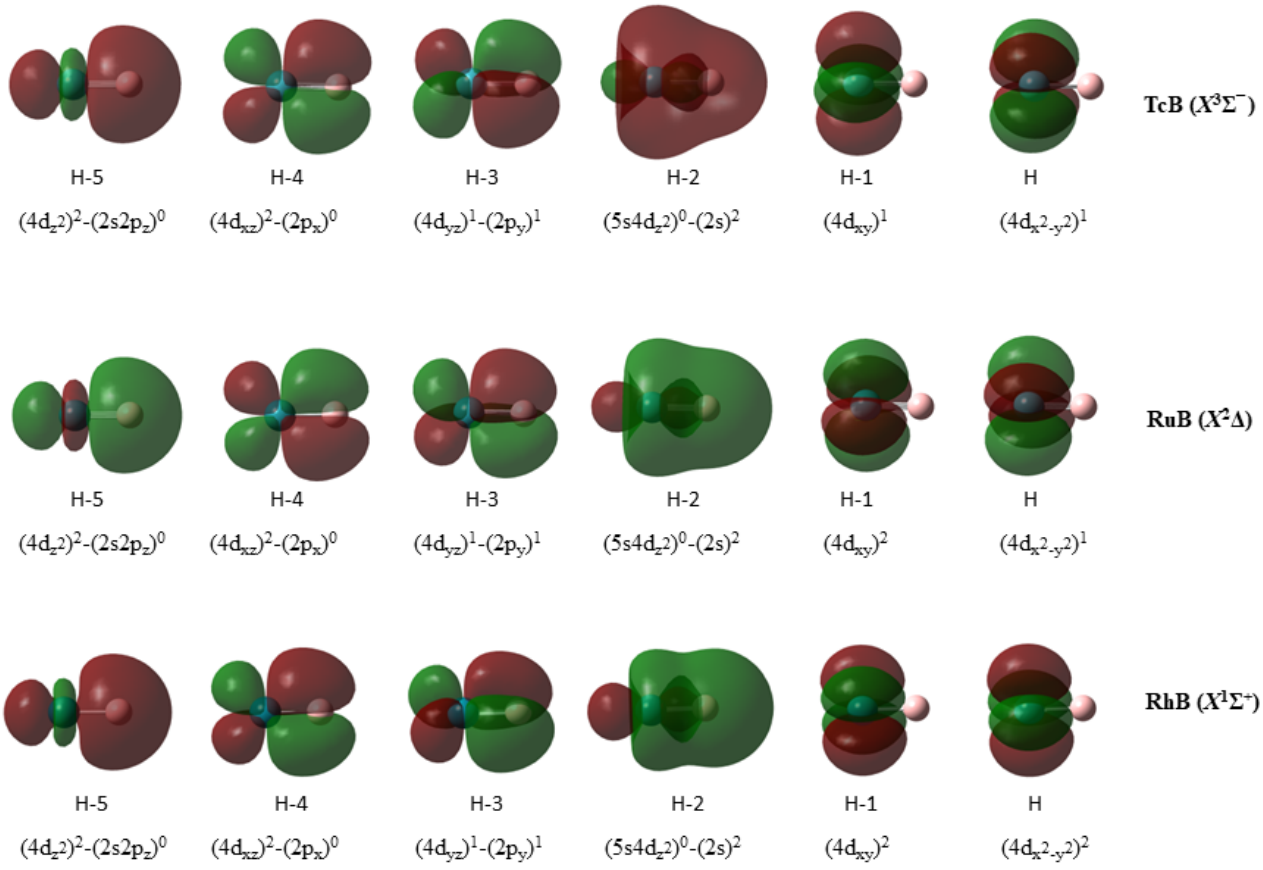

Figure 3. Molecular orbitals of the $X^3\Sigma^-$ (TcB), $X^2\Delta$ (RuB), and $X^1\Sigma^+$ (RhB) states presenting quadruple bonds.

4. Insights

Boron plays an important role in chemistry, biology, and materials science. Diatomic transition-metal borides are important building blocks of many complexes and materials and thus the knowledge of their dissociation energy, bond distances, and bonding analysis dipole moments is very useful. It is interesting that boron forms a variety of orders of bonding from single to quadruple bonds and bonds of different types, i.e., covalent, dative, and ionic bonds. In the present entry, the diatomic borides of transition metals are presented.

Three of them form quadruple bonds, i.e., RhB which was recently reported to form quadruple bonds [2][4], RuB and TcB form quadruple bonds in their ground states as well [21]. The X states of these three molecules present the same quadruple bonding, $\sigma^2\sigma^2\pi_x^2\pi_y^2$, and as the metal is escalated from Tc to Rh, the additional valence electron is added to the single occupied *d* orbitals, while the *X* states change from $X^3\Sigma^-$ (TcB) to $X^2\Delta$ (RuB) and then to $X^1\Sigma^+$ (RhB).

As a final remark, it has been reported that the states of the diatomic and triatomic molecules of sulfides are involved in complexes and solid or 2D-materials as building blocks, explaining the variety of their morphologies [19][20]. Similarly, the present data may provide a new approach to exploring the properties of solid state and 2D

metastable polymorphic materials involving transition-metal borides, while they may assist in explaining the catalytic properties of complexes, including transition-metal boride bonds.

References

1. Greenwood, N.; Earnshaw, A. Chemistry of the Elements, 2nd ed.; Butterworth-Heinemann: Oxford, UK, 1998.
2. Cheung, F.; Chen, T.-T.; Kocheril, G.S.; Chen, W.-J.; Czekner, J.; Wang, L.-S. Observation of Fourfold Boron-Metal Bonds in RhB(BO−) and RhB. J. Phys. Chem. Lett. 2020, 11, 659−663.
3. Shaik, ; Danovich, D.; Wu, W.; Su, P.; Rzepa, H.S.; Hiberty, P.C. Quadruple Bonding in C2 and Analogous Eight-Valence Electron Species. Nat. Chem. 2012, 4, 195−200.
4. Tzeli, ; Karapetsas, I. Quadruple Bonding in the Ground and Low-Lying Excited States of the Diatomic Molecules TcN, RuC, RhB, and PdBe. J. Phys. Chem. A 2020, 124, 6667–6681.
5. Tzeli, Quadruple chemical bonding in the diatomic anions TcN^{-}, RuC^{-}, RhB^{-}, and $PdBe^{-}$. J. Comput. Chem. 2021, 42, 1126–1137.
6. Ganem, ; Osby, J.O. Synthetically useful reactions with metal boride and aluminide catalysts. Chem. Rev. 1986, 86, 763–780.
7. Will, Electron deformation density in titanium diboride chemical bonding in TiB2. J. Solid State Chem. 2004, 177, 628–631.
8. Choi, J.; Roundy, D.; Sun, H.; Cohen, M.L.; Louie, S.G. The origin of the anomalous superconducting properties of MgB(2). Nature 2002, 418, 758–760.
9. Chung, ; Weinberger, M.B.; Levine, J.B.; Kavner, A.; Yang, J.; Tolbert, S.H.; Kaner, R.B. Synthesis of Ultra-Incompressible Superhard Rhenium Diboride at Ambient Pressure. Science 2007, 316, 436–439.
10. Wdowik, D.; Twardowska, A.; Rajchel, B. Vibrational Spectroscopy of Binary Titanium Borides: First-Principles and Experimental Studies. Adv. Condens. Matter Phys. 2017, 18, 4207301.
11. Decker, F.; Kasper, J.S. The crystal structure of TiB. Acta Crystallogr. 1954, 7, 77–80.
12. Spear, E.; McDowell, P.; McMahon, F. Experimental evidence for the existence of the Ti3B4 phase. J. Am. Ceram. Soc. 1986, 69, C-4–C-5.
13. Viswanathan, ; Sundareswari, M.; Jayalakshmi, D.S.; Manjula, M. Fermi surface and hardness enhancement study on ternary scandium and vanadium-based borides by first principles investigation. Comput. Mater. Sci. 2019, 157, 107–120.

14. Zhang, ; Liu, D.; Zhao, Y.; Li, W.; Gao, Y.; Duan, M.; Hou, H. Physical Properties and Electronic Structure of Cr2B Under Pressure. Phys. Status Solidi B 2020, 258, 2000212.
15. Gou, ; Steinle-Neumann, G.; Bykova, E.; Nakajima, Y.; Miyajima, N.; Li, Y.; Ovsyannikov, S.V.; Dubrovinsky, L.S.; Dubrovinskaia, N. Stability of MnB2 with AlB2-type structure revealed by first-principles calculations and experiments. Appl. Phys. Lett. 2013, 102, 061906.
16. Panda, B.; Ravi Chandran, K.S. First principles determination of elastic constants and chemical bonding of titanium boride (TiB) on the basis of density functional theory. Acta Mater. 2006, 54, 1641–1657.
17. Li, ; Zhou, R.; Cheng Zeng, X. Computational Analysis of Stable Hard Structures in the Ti-B System. Appl. Mater. Interfaces 2015, 7, 15607–15617.
18. Wang, ; Liu, C.; Wen, M.; Li, Q.; Ma, Y. Investigations on structural determination of semi-transition-metal borides. Phys. Chem. Chem. Phys. 2017, 19, 31592–31598.
19. Tzeli, ; Karapetsas, I.; Merriles, D.M.; Ewigleben, J.C.; Morse, M.D. The molybdenum-sulfur bond: Electronic structure of low-lying states of MoS. J. Phys. Chem. A 2022, 126, 1168–1181.
20. Mermigki, A.; Karapetsas, I.; Tzeli, D. Electronic structure of low-lying states of triatomic MoS2 molecule: The building block of 2D MoS2. Chem. Phys. Chem. 2023, 24, e202300365.
21. Demetriou, C.; Tzeliou, C.E.; Androutsopoulos, A; Tzeli, D. Electronic Structure and Chemical Bonding of the First-, Second-, and Third-Row-Transition-Metal Monoborides: The Formation of Quadruple Bonds in RhB, RuB, and TcB. Molecules 2023, 28, 8016.
22. Tzeli, ; Mavridis, A. Electronic structure and bonding of the 3D–transition metal borides, MB, M = Sc, Ti, V, Cr, Mn, Fe, Co, Ni, and Cu through all electron ab initio calculations. J. Chem. Phys. 2008, 128, 034309.
23. Merriles, M.; Tieu, E.; Morse, M.D. Bond dissociation energies of FeB, CoB, NiB, RuB, RhB, OsB, IrB, and PtB. J. Chem. Phys. 2019, 151, 044302.
24. Chi, ; Wang, J.-Q.; Hu, H.-S.; Zhang, Y.-Y.; Li, W.-L.; Meng, L.; Luo, M.; Zhou, M.; Li, J. Quadruple bonding between iron and boron in the BFe(CO)3− complex. Nat. Commun. 2019, 10, 4713.
25. Sevy, ; Huffaker, R.F.; Morse, M.D. Bond Dissociation Energies of Tungsten Molecules: WC, WSi, WS, WSe, and WCl. J. Phys. Chem. A 2017, 121, 9446−9457.
26. Merriles, M.; Nielson, C.; Tieu, E.; Morse, M.D. Chemical Bonding and Electronic Structure of the Early Transition Metal Borides: ScB, TiB, VB, YB, ZrB, NbB, LaB, HfB, TaB, and WB. J. Phys. Chem. A 2021, 125, 4420–4434.